Project 2

Alex Dombos, Samuel Lipschutz, Charles Loelius

2/5/14

1 DERIVATIONS

1.1

Outside the finite range R_n of the nuclear potential, the wave function expressed in terms of partial waves is

$$\psi(R, \theta) \overset{R \gtrsim R_n}{\to} \frac{1}{kR} \sum_{L=0}^{\infty} (2L+1)\, i^L P_L\left(\cos(\theta)\right) A_L \left[H_L^-(0, kR) - S_L H_L^+(0, kR) \right]$$

We also know that the asymptotic form of the wave function is comprised of an incoming plane wave (which is decomposed into partial waves) and outgoing spherical waves

$$\begin{aligned}
\psi^{\text{asym}}(R, \theta) &= e^{ikz} + f(\theta)\frac{e^{ikR}}{R} \\
&= \sum_{L=0}^{\infty}(2L+1)i^L P_L(\cos(\theta))\frac{1}{kR}\frac{i}{2}\left[H_L^-(0, kR) - H_L^+(0, kR)\right] + f(\theta)\frac{e^{ikR}}{R}
\end{aligned}$$

Equating these two expressions gives

$$\psi(R > R_n, \theta) = \psi^{\text{asym}}$$

$$\frac{1}{kR}\sum_{L=0}^{\infty}(2L+1)\,i^L P_L(\cos(\theta))\,A_L\left[H_L^-(0,kR) - S_L H_L^+(0,kR)\right] = \sum_{L=0}^{\infty}(2L+1)i^L P_L(\cos(\theta))\frac{1}{kR}\frac{i}{2}\left[H_L^-(0,kR) - H_L^+(0,kR)\right] + f(\theta)\frac{e^{ikR}}{R}$$

$$(kR)\left\{\frac{1}{kR}\sum_{L=0}^{\infty}(2L+1)\,i^L P_L(\cos(\theta))\,A_L\left[H_L^-(0,kR) - S_L H_L^+(0,kR)\right]\right\} = (kR)\left\{\sum_{L=0}^{\infty}(2L+1)i^L P_L(\cos(\theta))\frac{1}{kR}\frac{i}{2}\left[H_L^-(0,kR) - H_L^+(0,kR)\right] + f(\theta)\frac{e^{ikR}}{R}\right\}$$

$$\sum_{L=0}^{\infty}(2L+1)\,i^L P_L(\cos(\theta))\,A_L\left[H_L^-(0,kR) - S_L H_L^+(0,kR)\right] = \sum_{L=0}^{\infty}(2L+1)i^L P_L(\cos(\theta))\frac{i}{2}\left[H_L^-(0,kR) - H_L^+(0,kR)\right] + kf(\theta)e^{ikR}$$

$$\sum_{L=0}^{\infty}(2L+1)\,i^L P_L(\cos(\theta))\,A_L\left[i^L e^{-ikR} - S_L i^{-L} e^{ikR}\right] = \sum_{L=0}^{\infty}(2L+1)i^L P_L(\cos(\theta))\frac{i}{2}\left[i^L e^{-ikR} - S_L i^{-L} e^{ikR}\right] + kf(\theta)e^{ikR}$$

The asymptotic forms of the Hankel functions were used in the last step. Now the terms with e^{ikR} and e^{-ikR} factors are collected together separately.

$$e^{ikR}\left[\sum_{L=0}^{\infty}(2L+1)i^L P_L(\cos(\theta))\left\{A_L S_L i^{-L} - \frac{i}{2}i^{-L}\right\} + kf(\theta)\right] = e^{-ikR}\left[\sum_{L=0}^{\infty}(2L+1)i^L P_L(\cos(\theta))\left\{A_L i^L - \frac{i}{2}i^L\right\}\right]$$

Since the expressions in the square brackets are independent of R, and $e^{\pm ikr}$ are linearly independent, the expressions in the square brackets must equal zero independently. Also, due to the orthogonality of the Legendre Polynomials, for the second expression in the square brackets to be zero for all L, then each term in the sum must be zero. This means $A_L = i/2$.

Using $A_L = i/2$ in the first term gives

$$e^{ikR}\left[\sum_{L=0}^{\infty}(2L+1)i^L P_L(\cos(\theta))\left\{A_L S_L i^{-L} - \frac{i}{2}i^{-L}\right\} + kf(\theta)\right] = 0$$

$$\Rightarrow \left[\sum_{L=0}^{\infty}(2L+1)i^L P_L(\cos(\theta))\left\{\left(\frac{i}{2}\right)S_L i^{-L} - \frac{i}{2}i^{-L}\right\} + kf(\theta)\right] = 0$$

$$\Rightarrow \sum_{L=0}^{\infty}(2L+1)i^L P_L(\cos(\theta))\left(\frac{i}{2}i^{-L}\right)(S_L - 1) = -kf(\theta)$$

$$\Rightarrow \left(\frac{i}{2}\right)\left(\frac{-1}{k}\right)\left(\frac{i}{i}\right)\sum_{L=0}^{\infty}(2L+1)P_L(\cos(\theta))(S_L - 1) = f(\theta)$$

$$\Rightarrow f(\theta) = \frac{1}{2ik}\sum_{L=0}^{\infty}(2L+1)P_L(\cos(\theta))(S_L - 1)$$

1.2

The scattering amplitude can be written as

$$f(\theta) = \frac{1}{2ik} \sum_{L=0}^{\infty} (2L+1)P_L(\cos(\theta))(S_L - 1)$$

$$= \frac{1}{2ik} \sum_{L=0}^{\infty} (2L+1)P_L(\cos(\theta)) \left[e^{2i\delta_L} - 1 \right]$$

$$= \frac{1}{2ik} \sum_{L=0}^{\infty} (2L+1)P_L(\cos(\theta)) \left[e^{i\delta_L} (e^{i\delta_L} - e^{-i\delta_L}) \right]$$

$$= \frac{1}{2ik} \sum_{L=0}^{\infty} (2L+1)P_L(\cos(\theta)) \left[2ie^{i\delta_L} \sin(\delta_L) \right]$$

$$= \frac{1}{k} \sum_{L=0}^{\infty} (2L+1)P_L(\cos(\theta)) e^{i\delta_L} \sin(\delta_L)$$

Using this, the total elastic cross section for neutrons is

$$\sigma_{\text{el}} = \int |f(\theta)|^2 d\Omega$$

$$= \int_0^{2\pi} d\phi \int_0^{\pi} |f(\theta)|^2 \sin(\theta) d\theta$$

$$= \int_0^{2\pi} d\phi \int_0^{\pi} \left[\frac{1}{k} \sum_{L'=0}^{\infty} (2L'+1)P_{L'}(\cos(\theta))e^{i\delta_{L'}}\sin(\delta_{L'}) \right]^* \left[\frac{1}{k} \sum_{L=0}^{\infty} (2L+1)P_L(\cos(\theta))e^{i\delta_L}\sin(\delta_L) \right] \sin(\theta) d\theta$$

$$= \frac{2\pi}{k^2} \sum_{L'=0}^{\infty} \sum_{L=0}^{\infty} (2L'+1)(2L+1)e^{-i\delta_{L'}}\sin(\delta_{L'})e^{i\delta_L}\sin(\delta_L) \left[\int_0^{\pi} P_{L'}(\cos(\theta))P_L(\cos(\theta))\sin(\theta) d\theta \right]$$

$$= \frac{2\pi}{k^2} \sum_{L'=0}^{\infty} \sum_{L=0}^{\infty} (2L'+1)(2L+1)e^{-i\delta_{L'}}\sin(\delta_{L'})e^{i\delta_L}\sin(\delta_L) \left[\frac{2}{2L+1}\delta_{LL'} \right]$$

$$= \frac{2\pi}{k^2} \sum_{L'=0}^{\infty} (2L'+1)(2L'+1)e^{-i\delta_{L'}}\sin(\delta_{L'})e^{i\delta_{L'}}\sin(\delta_{L'})\frac{2}{2L'+1}$$

$$= \frac{4\pi}{k^2} \sum_{L'=0}^{\infty} (2L'+1)\sin^2(\delta_{L'})$$

Relabeling L' to L gives the desired result

$$\sigma_{\text{el}} = \frac{4\pi}{k^2} \sum_{L=0}^{\infty} (2L+1)\sin^2(\delta_L)$$

1.3

If considering proton scattering instead of neutron scattering, the Coulomb interaction must be included in the calculation of the elastic scattering phase shift. The Coulomb interaction is included by modifying the asymptotic forms of the Hankel functions,

3

$H_L^{\pm}$. The asymptotic form of the Hankel functions are now $H_L^{\pm}(\eta, \rho) \sim e^{i\Theta}$ where $\Theta = \left[\rho - L\frac{\pi}{2} + \sigma_L(\eta) - \eta \ln(2\rho)\right]$ and $\sigma_L(\eta) = \arg\Gamma(1 + L + i\eta)$ is the Coulomb phase shift. The infinite range of the Coulomb potential is reflected in the term $\ln(2\rho)$, which never goes away for large ρ.

2 TARGET SELECTION

In this case, we consider the setup to be a target of stable ^{58}Ni, in its ground state. We thereby find that we have quantum numbers in the entrance partition corresponding to (assuming neutron/proton scattering):

Table 2.1: Table of Quantum Values

Quantum Number	Value
Mass partition x	T=58,P=1
Charge	28
Spin	0
Parity	+

3 POINTLIKE AND STRUCTURED COULOMB SCATTERING

We would expect, in the absence of any nuclear forces, and for a point like nucleus, that that the proton would have a pure Rutherford cross section. Upon taking into account the finite size of the target, we recognize that there is a perturbation in the distribution of charge, so that the electric potential will switch from a $\frac{1}{r}$ term to a linear term proportional to r. We expect that this should mean that at energies high enough to probe the structure of the proton-i.e. those that can overcome the Coulomb potential to have a reasonably large wavefunction in the vicinity of the proton- there ought to be an increased cross section in the forward direction.

We compare this below to four graphs of the Coulomb potential, one pointlike and one with spatial extent, with energies of .1 MeV and 50 MeV.

We see that this is exactly what was anticipated, that the pointlike Coulomb scattering is indentical to the Rutherford cross section, whereas the case where the target (Nickel 58) has a radial extent shows no structure for low energy projectiles but has the expected forward peaking for high energy.
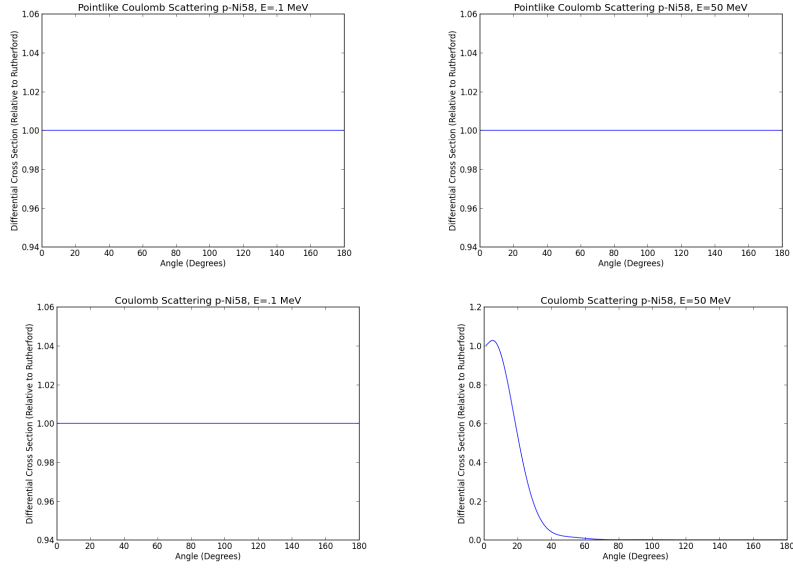
Figure 3.1: Comparison of Pointlike (top) and Extended (bottom) Coulomb Cross Sections

4 Proton-Nickel Analysis

4.1 Differential Cross Sections

Here we examine the cross sections for the case of proton scattering on ^{58}Ni with an optitcal potential paramaterized into volume, surface and spin-orbit components. Below in figure 6.1 we have the full potential (left) and only the real terms included (right). In all cases we see the cross section (plotted vs. the Rutherford cross section) approach 1 at 0 degrees. This is expected as the Coulomb component diverges strongly at 0 degrees and should dominate. For the case of 5 MeV protons we see only small deviations away from the Rutherford cross section, since at this energy the Coulomb barrier is shielding the details of the optical potential.
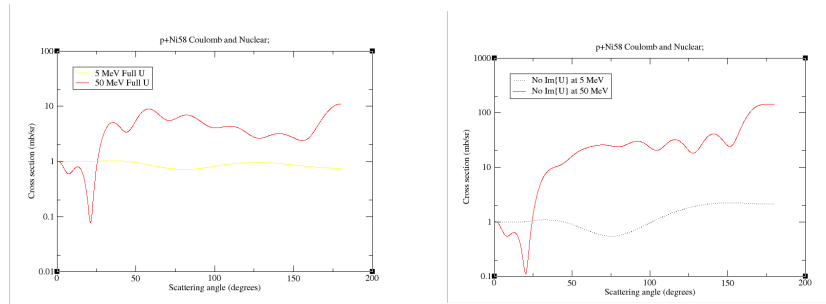

Figure 4.1: Differential Cross Sections for Proton Interactions

Below in figure 6.2 we have a comparision of the cross section with and without the imaginary part of the potential. Seen in both the 5 MeV and 50 MeV cases the overall strength is reduced for the potential containing imaginary components. This is expected as the loss of flux created by the imgainary potential should lower the probability of elastic scatterings.
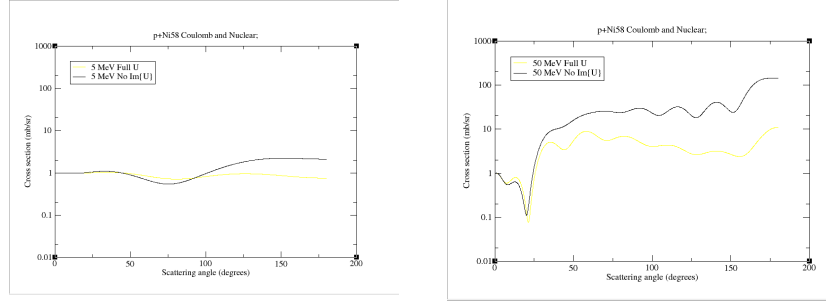

Figure 4.2: Differential Cross Sections for Proton Interactions

4.2 S-Matrix Components

Below in figure 6.3 we have the modulus of the S-Matrix vs. total J. As one expects, the case where there is no imaginary component of the potential all the values are 1. Without a loss of flux the S-Matrix must be unitary. In the opposing case there is strong deviation from 1 for the lower partial waves. Further it is seen that the values quickly converge around $L = 10$, and despite this we have calculated all the way out to $L = 100$.
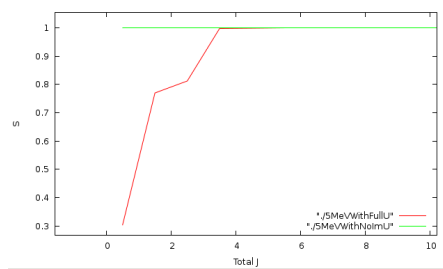

Figure 4.3: Modulus of the S-Matrix values as a function of J

4.3 Increased Radii and Diffusiveness

Below in figure 6.4 the cross sections for different radii and diffuseness parameters are compared. In both cases the values were increased by a factor of 1.5 in all the terms of the potential (volume, surface and spin-orbit). On the left is the increased radius case. Here the 5 MeV protons move farther from the pure Rutherford case as the extent of the nuclear interaction has been increased. We see this also in the 50 MeV case where

6

the overall trend tends to be amplified. On right we have the increased diffuseness case. Here we again see more deviation from pure Rutherford for the 5 MeV protons, but we also see a decrease in the backward angles. If we had decreaed the diffuseness, making the potential more like a delta funcion, then we would expect there to be an increase in the backward angles. As it becomes more diffuse there are more ways to scatter to foward angles, causing a decrease in backward angles.
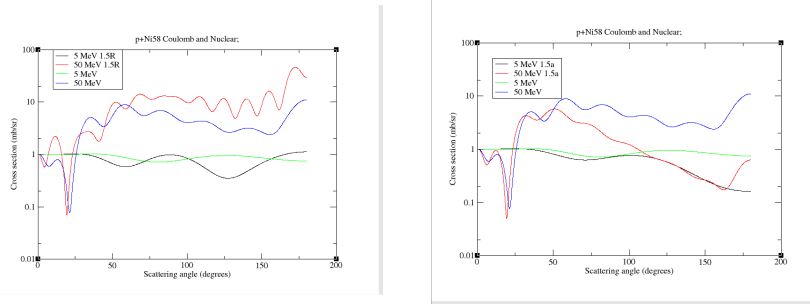

Figure 4.4: Comparison of increased Radii (left) and diffuseness (right) to original potential values

5 Neutron-Nickel Analysis

5.1 Differential Cross Sections

We then consider the previous analysis using a similar potential model for the nuclear optical potential, but setting the charge of the projectile to 0, and changing the optical potential to be for n-scattering as found in Reference 2 below. The results of this are plotted below.
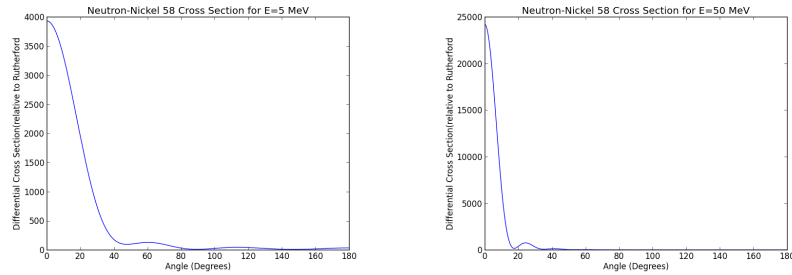

Figure 5.1: Differential Cross Sections for Neutron Interactions

We can see in this case that the distributions are sharply peaked near zero, with the major difference being in the extreme sharpness of the 50 MeV compared to a somewhat broader peak for the 5 MeV. This makes sense because in the absence of a Coulomb

interaction, the only potential is the optical potential. Since the 50 MeV neutron has a larger energy compared to the optical potential and so is less affected. However, the 5 MeV neutron, no longer prevented from interacting with the optical potential due to the Coulomb force, is likely to interact more with the optical potential. This explains the broader scattering. We might expect something similar as energy decreases and the optical potential causes further interactions. However, this must be reconciled with an expected decrease in flux caused by increase interactions with the imaginary potential.

5.2 Increased Diffuseness

In this case, I have set the diffuseness parameter to be ten times larger than in the standard found in the previous optical potential. This results in a cross section as follows (for 5 MeV):
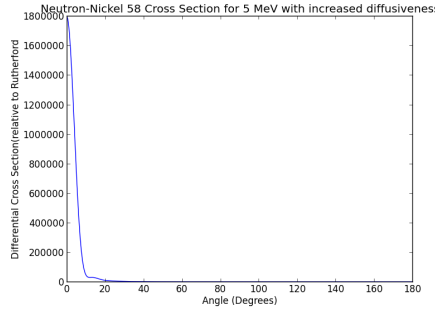
We see that for increased diffusiveness that the forward cross section becomes nearly infinite, in comparison to the Rutherford cross section, which follows because at a near infinitely large diffusive constant the potential is nearly zero in any area and so has no effect on the trajectory. Thus the particle will continue unperturbed, and so have a scattering angle of 0. As such it follows that this will be much larger than the Rutherford cross section which in principle should allow for no such scattering. What's more, the diffuseness means the imaginary potential absorbs less and so the cross section becomes much larger.

5.3 Increased Radius

In this case we consider a radius parameter in the optical potential to also be ten times larger than in the potential defined above. This has the effect of increasing the range over which the potential is strong, and so increases the overall effect of the potential, leaving a larger relative amount of the cross section over which to be scattered. However, it also increases the surface area and volume, which means that there is an increased probability for absorption through the imaginary potential and so an overall smaller cross section.
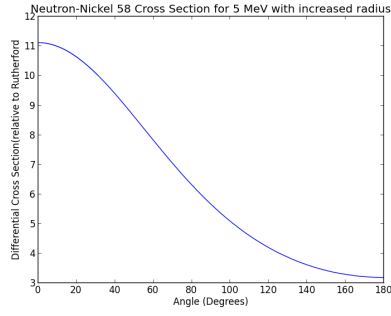
5.4 DIFFERENT STRENGTH OF IMAGINARY POTENTIALS

We then ought to anticipate a difference in the total cross sections and so the elastic differential cross sections of the potential, and so a strong imaginary potential(in this case multiplied by ten from the above) ought to have a much smaller cross section than that of the weak potential(in this case wth the strength of the imaginary potentials divided by ten.)
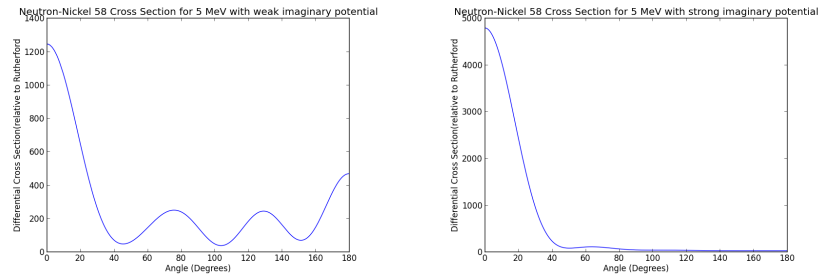These are plotted below:

Figure 5.2: Differential Cross Sections for Neutron-Ni58 with Varying Imaginary Potentials

We note that in this instance we don't seem to have the same agreement expected, as it would appear that there is a larger cross section with the strong imaginary potential. However, instead we should look at the modul of the S matricesi for different L states, which will show the overall absorption. These are plotted below:

Here we see clearly that especially at low angular momenta the strong imagnary potential starts with a much smaller S matrix than that of the weak, and only slowly converges to 1 with a large L.
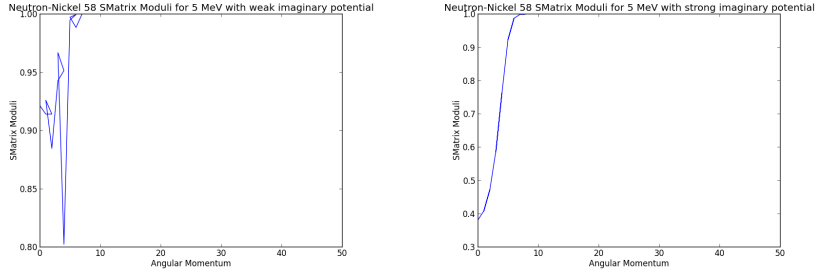
Figure 5.3: Moduli of S for Neutron-Ni58 with Varying Imaginary Potentials

6 TOTAL CROSS SECTIONS

We return to the five and fifty MeV neutron-Ni58 scattering previously examined, note that in the output files generated there is in fort.40 a description of the cross sections. We plot the results in the table below:

Energy (MeV)	Reaction (mbarns)	Elastic (mbarn)	Total (mbarn)
5	2262	1802	4064
50	1548	1889	3437

Table 6.1: Table of Cross Sections

And in this we see that the high energy neutron has a lower overall cross section, primarily driven by an increased lack of reactions as the potential is unable to affect the high energy neutron much.

7 POTENTIAL REFERENCES

7.1 PROTONS

A. J. Koning, J. P. Delaroche, Nucl. Phys. A713, 231 (2003). Using the Reference Input Parameter Library, this corresponds to the OMP index of 4421. The specific URL is `https://www-nds.iaea.org/cgi-bin/ripl_om_param.pl?Z=28&A=58&ID=4421&E1=0.1&E2=150`.

7.2 NEUTRONS

A. J. Koning, J. P. Delaroche, Nucl. Phys. A713, 231 (2003). Using the Reference Input Parameter Library, this corresponds to the OMP index of 4117. The specific URL is `https://www-nds.iaea.org/cgi-bin/ripl_om_param.pl?Z=28&A=58&ID=1417&E1=0.1&E2=150`.